Local Structure of Core–Shell MnFe 2 O 4+δ -Based Nanocrystals: Cation Distribution and Valence States of Manganese Ions

Fernando H. Martins, Franciscarlos G. Silva, Fábio L. O. Paula, Juliano de A. Gomes, Renata Aquino, José Mestnik-Filho, Pierre Bonville, Florence Porcher, Régine Perzynski, Jérôme Depeyrot

THE JOURNAL OF PHYSICAL CHEMISTRY C

Article

pubs.acs.org/JPCC

Local Structure of Core–Shell $MnFe_2O_{4+\delta}$-Based Nanocrystals: Cation Distribution and Valence States of Manganese Ions

Fernando H. Martins,[†,‡] Franciscarlos G. Silva,[†,¶] Fábio L. O. Paula,[†] Juliano de A. Gomes,[§] Renata Aquino,[¶,†] José Mestnik-Filho,[∥] Pierre Bonville,[⊥] Florence Porcher,[#] Régine Perzynski,[‡] and Jérôme Depeyrot*[,†]

[†]3NANO Group, Laboratório de Fluidos Complexos, Instituto de Física, Universidade de Brasília, UnB, 70919-970 Brasília-DF, Brazil

[‡]Sorbonne Universités, UPMC Univ Paris 06, CNRS, Lab. PHENIX, 4 Place Jussieu, 75005 Paris, France

[¶]3NANO Group, Laboratório de Nanociência Ambiental e Aplicada-LNAA, Universidade de Brasília, UnB, 73345-010 Brasília-DF, Brazil

[§]Instituto de Criminalística, Polícia Civil do Distrito Federal, 70610-200 Brasília-DF, Brazil

[∥]Instituto de Pesquisas Energéticas e Nucleares, Av. Prof. Lineu Prestes 2242, 05508-000 São Paulo-SP, Brazil

[⊥]Service de Physique de l'État Condensé, CEA, CE Saclay, DSM/IRAMIS/SPEC/LNO, 91191 Gif-sur-Yvette Cedex, France

[#]Laboratoire Léon Brillouin UMR 12 CEA/CNRS Bâtiment 563, Centre d'Etudes Nucléaires CEA/Saclay, 91191 Gif-sur-Yvette Cedex, France

S *Supporting Information*

ABSTRACT: We investigate the local structure of nanoparticles based on a manganese ferrite core surrounded or not by a maghemite layer obtained after hydrothermal surface treatment. Results of X-ray powder diffraction (XRD) and neutron powder diffraction (NPD) measurements are crossed with those of in-field Mössbauer spectroscopy and X-ray absorption spectroscopy (XANES/EXAFS) to study the valence state of Mn ions and the cation distribution at interstitial sites of the core–shell nanoparticle structure. Linear combination fitting of XANES data clearly indicates the existence of mixed valence states of Mn cations in the Mn ferrite phase. As a direct consequence, it induces nonequilibrium cation distributions in the nanoparticle core with the presence of a large amount of Mn cations at octahedral sites. The quantitative results of the inversion degree given by NPD, Mössbauer spectroscopy measurements, and EXAFS are in good accordance. It is also shown that both the proportions of each oxidation degree of Mn ions and their location at tetrahedral or octahedral sites of the spinel nanocrystal core can be modified by increasing the duration of the surface treatment.

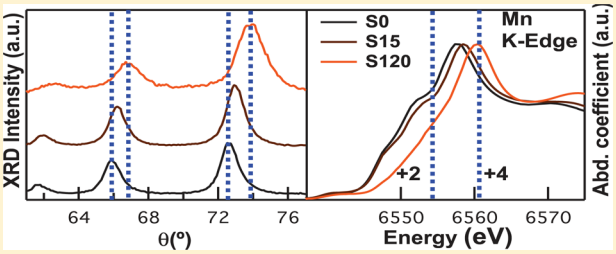

INTRODUCTION

Among the nanomaterials, magnetic nanoparticles (NPs) have gained a lot of interest for many years because of their peculiar chemical and physical properties.[1] This considerable attention is mainly due to their applicability in several areas such as catalysis,[2] magnetic data recording,[3] and biomedicine.[4−6] More specifically, manganese ferrite ($MnFe_2O_4$) NPs could be very good candidates for these applications because they are well-known for their soft magnetic properties with high electrical resistance and magnetic permeability, good chemical stability, mixed valence states, low coercivity, and moderate magnetic saturation.[7−9] As an example, for the production of hydrogen as a clean and renewable energy resource, they are used in the nanoscale design of new catalysts for thermochemical water splitting.[10] For biomedical applications, approaches that combine both therapeutic and diagnostic use in only one multifunctional particle constitute a crucial challenge, markedly in the case of cancer treatment. As an example, $MnFe_2O_4$ NPs have been extensively investigated for the detection of tumors, as contrast agents in magnetic resonance imaging, and in the definition of damages zones in local edemas.[11−14] They also present high specific loss power (SLP), low inherent toxicity, uptake efficiency, and fast thermal response, which make them selected materials for controlled magnetic hyperthermia.[15,16]

Using heterogeneous nanostructures, that is, core–shell magnetic NPs (CS-NPs), different properties can be combined in a unique object, which may contribute to the fine-tuning of their physical and chemical properties, leading therefore to improvement of the whole of their performances. Regarding the magnetic anisotropy, associations of hard and soft phases in the core or in the shell of the magnetic nanostructures have been proposed.[3,17] In recent work concerning CS-NPs of

Received: September 13, 2016
Revised: March 27, 2017
Published: March 28, 2017

DOI: 10.1021/acs.jpcc.6b09274
J. Phys. Chem. C 2017, 121, 8982−8991

Table 1. Characteristics of $MnFe_2O_4$-Based NPs Investigated in This Work[a]

sample	time of treatment (min)	χ_M	D_{XR}(nm)	ϕ_c/ϕ	t_{sh} (nm)	$\langle a \rangle$ (nm)
S0		0.33(1)	10.9(1)	1		0.845(3)
S15	15	0.25(2)	10.7(1)	0.75(2)	0.6(1)	0.842(1)
S120	120	0.18(1)	8.1(1)	0.53(1)	0.9(1)	0.834(3)

[a]χ_M is the molar fraction of manganese ions obtained by ICP and AAS techniques, $\langle a \rangle$ is the average lattice parameter deduced from Bragg's law, ϕ_c/ϕ is the volume fraction of the core, and t_{sh} is the thickness of the surface layer. The particle sizes (D_{XR}) were obtained by Scherrer's equation.

$MnFe_2O_4@\gamma$-Fe_2O_3 and $CoFe_2O_4@\gamma$-Fe_2O_3, the magnetic exchange coupling between soft or hard ferrite cores and a maghemite (γ-Fe_2O_3) shell has been measured.[18] This coupling, larger for CS-NPs made of more anisotropic cores, would give larger SLP values, thus improving the efficiency of the conversion of the electromagnetic energy into heat.[19] As the magnetic anisotropy and the NP magnetization are structure-dependent for both the core and the shell, satisfactory knowledge of the detailed structure in such nanocrystals has become the subject of primary interest for understanding their behavior in biomedical and technological applications.

An ideal manganese ferrite spinel structure, generally produced at high temperatures by solid-state reactions or ceramic methods[20,21] as well as by laser ablation deposition,[22,23] presents an inversion degree of around 0.2, similar to that encountered for bulk materials. Nevertheless, manganese ferrite NPs prepared at lower temperatures, by soft chemistry routes such as hydrothermal coprecipitation,[24−26] thermal decomposition of metal carbonyl complexes,[27] reverse micelle synthesis,[28] or sol−gel methods,[16,21] and also those prepared by ball milling[29] often present a nonequilibrium cation distribution. The inversion degree in these nanomaterial has been successfully determined in manganese ferrite NPs and thin films by means of techniques such as X-ray absorption,[20,21,24,26,28] diffraction anomalous fine structure,[22,23] X-ray magnetic circular dichroism,[30] in-field Mössbauer spectroscopy,[26,29] and neutron powder diffraction (NPD).[25]

The study of cation inversion in $MnFe_2O_4$ NPs is mainly related to investigations of the Néel temperature, an issue that has been controversial during the last 2 decades.[31−33] Enhanced measured values were first attributed to a finite size scaling effect. Since then, several studies have unambiguously demonstrated the dominant role played by cation redistribution, owing to increased superexchange interactions when a transfer of a fraction of Fe ions occurs from B sites to A sites as a result of cationic exchange with Mn ions.[16,26,32,34] The site preference of Mn ions for octahedral coordination is clearly associated with its oxidation state because Mn^{3+} ions present a higher crystal field stabilization energy when located at B sites.[21,24,34] Several factors would increase the chances to promote the oxidation of Mn ions, among them, the use of highly basic solutions in modified coprecipitation methods and calcination in air at much higher temperatures.[21,25] Then, various values of the inversion degree were found, ranging from 0.2 (the ideal bulk value) to 0.7, larger values always related to a larger proportion of Mn ions with higher valence states.

We are currently working on the synthesis of core−shell ferrite NPs and on their colloidal dispersion in acidic and neutral media in order to obtain ferrofluids.[35,36] In previous works, a nonequilibrium cation distribution among interstitial sites of CS-NPs based on zinc ferrite cores suggested a spinel-type nanocrystal structure.[37,38] Cation redistribution takes place during the coprecipitation step without altering the long-range structural order of the whole of these nanocrystals. The number of Zn^{2+} ions located at octahedral sites of the zinc ferrite core does not change after surface treatment and is independent of the size of the particles. The interatomic distances are very close to those obtained for reference bulk materials but are not affected by protective surface treatment nor by size reduction. Moreover, the average coordination number found for metallic cations decreases for surface iron atoms and is much less affected for the "screened" Zn cations of the NP core.

In such a context, a careful investigation of $MnFe_2O_{4+\delta}@\gamma$-$Fe_2O_3$ CS-NPs is proposed here, in order to investigate the cation distribution and the valence state of the Mn ion as a function of the surface treatment duration. These nanomaterials present an important magnetic disorder, mainly localized in the surface shell, which progressively freezes in a spin-glass-like state at very low temperatures.[39] Then, when cooled under a field, the surface spins are pinned and therefore become the source of exchange bias anisotropy for the uniformly magnetized core. This pinning effect has been pointed out to enlighten in such $MnFe_2O_4@\gamma$-Fe_2O_3 CS-NPs intra- and interparticle exchange bias.[40] For these reasons also, a clear understanding of the internal atomic arrangement of these CS-NPs is necessary.

MATERIALS AND METHODS

$MnFe_2O_{4+\delta}@\gamma$-$Fe_2O_3$ CS-NPs were synthesized according to our previously reported coprecipitation method;[35,38,41−43] a detailed synthesis procedure is covered in the SI. The products were characterized by inductively coupled plasma atomic emission spectroscopy (ICP-AES) or atomic absorption spectroscopy (AAS), X-ray powder diffraction (XRD), NPD, X-ray absorption near edge structure (XANES), extended X-ray absorption fine structure (EXAFS), and Mössbauer spectroscopy. For more details regarding characterization, see the SI.

RESULTS

A. Chemical Titration and XRD: CS-NP Characteristics.

The effects of hydrothermal superficial treatment on the coprecipitated NPs have been extensively described in ref 35. It consists first of a release of miscoordinated divalent metal from the NP surface and second of incorporation of iron in a superficial layer of maghemite onto the NP core. It has been shown that the thickness of the shell increases with the decrease of particle size and depends on the underlying ferrite in equivalent conditions of synthesis. Moreover, the quantity of incorporated iron ions increases as the heating time increases. The results collected in Table 1 typically illustrate the core−shell formation and the influence of the treatment duration. The NPs obtained right after the coprecipitation step (S0 sample) are stoichiometric, and their molar fraction of manganese ions is therefore 0.33. After surface modification, the NPs are no longer chemically homogeneous. Molar fractions of manganese ions equal 0.25 after 15 min of treatment (S15) and 0.18 after 120 min of treatment (S120).

DOI: 10.1021/acs.jpcc.6b09274
J. Phys. Chem. C 2017, 121, 8982−8991

Figure 1 shows the XRD diffractograms obtained for the three samples. Using Bragg's law, each peak is indexed and

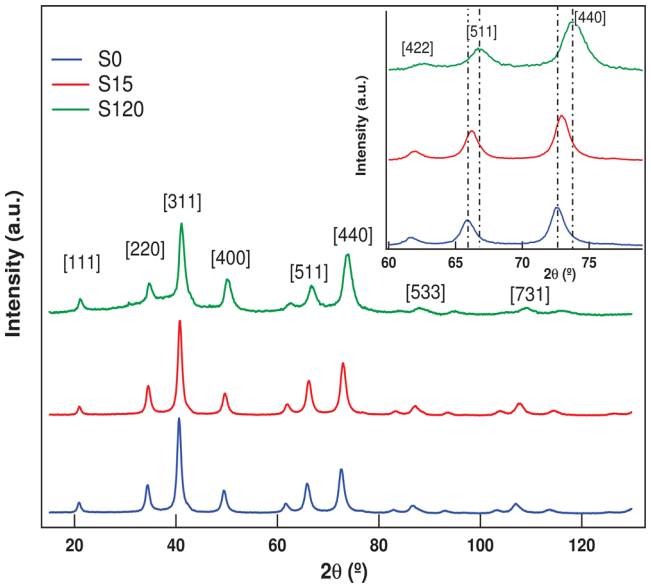

Figure 1. XRD pattern of manganese ferrite samples S0, S15, and S120. The beam intensity is plotted as a function of the scattering angle, 2θ, in degrees. λ = 1.77126 Å. (Inset) Amplification of the XRD pattern of manganese ferrite samples showing the shift of the diffraction peaks for bigger angles 2θ.

associated with an interplane spacing of the crystalline spinel-type nanostructure. The absence of other contributions indicates that there is no other crystalline structure besides the spinel, neither formed during the coprecipitation step nor induced by hydrothermal surface treatment. We first use the Scherrer formalism to evaluate the size of the CS-NPs from the broadening of the diffracted lines. We also calculate the volume fraction of each spinel phase from the metal concentrations obtained from chemical titrations. Then, from the maghemite shell fraction, which varies from 25% for S15 to 47% for S120, we evaluate the shell thickness. The typical values of the size D_{XR} and of the thickness t_{sh} of the maghemite surface layer are collected in Table 1. The shell thickness increases as the heating time increases, in good agreement with the conclusions of ref 35. From indexing of each diffractogram peak, the averaged parameter $\langle a \rangle$ of the cubic lattice is calculated, and its values are also listed in Table 1. We observe that the cell size of pure $MnFe_2O_4$ NPs (sample S0), found equal to 0.845 nm, is smaller than the cell size of ideal bulk materials, equal to 0.851 nm. Moreover, as displayed in the inset of Figure 1, when the duration of the surface treatment increases, each peak shifts toward larger diffraction angles, therefore indicating that the cubic cell size reduces with the treatment time (see the deduced values of the cell parameter in Table 1). Two effects might be considered to enlighten this result. One of them concerns the oxidation of Mn ions, which could easily occur when the NPs are coprecipitated in a highly basic medium.[25] Then, as has been observed in spinel-type NPs, the anion−cation distance is reduced, leading to a decrease of the cubic cell size.[9,34] Results of XANES measurements will be presented in the next subsection and will provide a clear answer to this question. The second effect is a direct consequence of the core−shell structure. The deduced lattice parameter is an average parameter that must take into account the inhomogeneous structure of the CS-NPs and the slight lattice mismatch at the interface. The cubic cell parameter is smaller for maghemite (0.835 nm), and as its proportion increases, the value encountered for the lattice parameter of the CS-NPs would be lower. In subsection E and the SI, a more detailed analysis of XRD data, based on Rietveld refinement considering two spinel phases, will provide quantitative results. However, let us first present XANES and EXAFS qualitative results in order to evidence the relation between the valence state of the manganese ions and the inversion degree.

B. X-ray Absorption Near Edge Spectroscopy (XANES). Figure 2 presents room-temperature XANES spectra

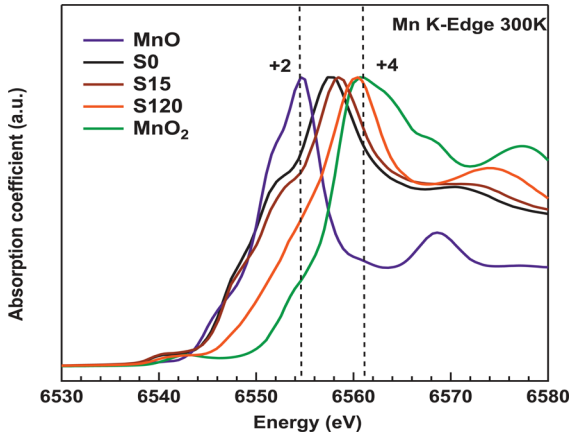

Figure 2. Experimental XANES spectrum of the manganese K-edge at room temperature of the reference materials and the NP samples. The shift observed for the spectrum, more significant for sample S120, is related to partial oxidation of the manganese cations in the structure.

at the Mn K-edge of samples S0, S15, and S120 together with those of MnO and MnO_2 reference oxides. We determine the mean oxidation state of Mn cations in the nanocrystal structure by comparing the absorption edge energy obtained for CS-NPs samples with those measured for both standard manganese oxide compounds. The energy of the absorption edge is commonly taken as the maximum of the first derivative of the normalized absorbance and generally corresponds to half of the absorption jump.[44,45] Nevertheless, here the XANES spectra of CS-NPs are found rich in structure, making this task more difficult. Then, in order to avoid misinterpretation on the value attributed to the edge energy $E0$ and to allow a careful comparison between all spectra, we set the edge energy position to the zero of the first derivative of the absorption amplitude (main peak position in the spectra displayed in Figure 2), as in refs 24 and 44. Figure 2 shows that the energy edge of each sample of CS-NPs is shifted to larger values when compared to that of the MnO reference, which presents an absorption peak centered at around 6554.7 eV, associated with the 2+ valence state. It indicates that the mean oxidation state of manganese ions in our CS-NPs is larger than 2+, the value expected for an ideal Mn ferrite structure.[20,21] A more detailed analysis leads to the energy of the central peak, located at 6557.7 eV for S0, 6558.4 eV for S15, and 6560.4 eV for S120. The latter value is very close to that of the absorption peak of MnO_2 located at 6561.0 eV and for which the Mn oxidation degree is 4+. As a shift of about 3 eV can be associated with a unit variation of the mean oxidation state,[24,44,45] such results show unambiguously that the hydrothermal surface treatment, which creates the core−shell nanostructure, also promotes the

DOI: 10.1021/acs.jpcc.6b09274
J. Phys. Chem. C 2017, 121, 8982−8991

oxidation of Mn cations. Simulations of XANES absorption spectra, performed within the linear combination fit (LCF) using reference oxide compounds, will enlighten our discussion in the next section. The absorption edge of our CS-NPs is also measured at the iron K-edge. For all NP samples, the mean oxidation state of iron ions in the nanocrystal structure was found to be around 3+.

We also note in Figure 2 the presence of a shoulder at around 6552 eV, well marked for S0 and S15 sample spectra. It is related to the Jahn−Teller effect, which results in an elastic distortion of the octahedral sites in order to energetically compensate rearrangement of the electronic distribution $t_{2g}e_g$ of octahedrally coordinated Mn^{3+} cations.[24,26] The intensity of this shoulder is lower for S120, which could indicate for this sample a lower proportion of Mn^{3+} cations at octahedral sites, probably due to partial oxidation of Mn^{3+} ions to Mn^{4+} ions occurring during surface treatment. This result is in good accordance with the observed reduction of the cubic cell size deduced from the shift of the X-ray characteristic peaks observed in the inset of Figure 1. Here also, the LCF calculations will help us to better understand the spectral behavior. In the following, Fourier-transformed EXAFS will confirm the effect of the surface treatment time on the manganese cation distribution and valence state.

C. Extended X-ray Absorption Fine Structure (EXAFS). The Fourier transform amplitude of S0, S15, and S120 samples has been extracted from EXAFS data recorded at the Mn K-edge at 100 K and is shown in Figure 3a for each sample. It has been obtained using the same parameters and can be thus represented in the same coordinate system, allowing direct comparison. All spectra exhibit two main contributions, which are always located at similar values of the radial distance. These very close local structures agree well with the extended crystalline arrangement of the NPs, found to be the same for all samples, as already pointed out by XRD data of Figure 1. The first contribution, centered at 1.4 Å, is associated with the first coordination shell of oxygen atoms around manganese cations. Careful observation indicates that it rather corresponds to the convolution of two peaks, one located at a short Mn−O distance (A sites) and another centered at a longer one (B sites).[9] We also see that the intensity of the latter increases at the expense of that of the former as the surface treatment time increases. It probably reflects a larger fraction of manganese cations coordinated in octahedral geometry according to a larger mean oxidation degree when the duration of the surface treatment increases. The amplitude of the whole peak related to the manganese first nearest neighbor also increases progressively from the S0 to S120 sample. It is related to an enhanced coordination number observed for Mn absorber cations of surface-treated NPs due to the formation of a core−shell structure. Indeed, it has already been shown that the performed hydrothermal treatment, which occurs in an acidic solution of ferric nitrate, removes undercoordinated divalent cations and incorporates more iron ions in the NPs' surface shell.[35] Therefore, a smaller mean coordination number is observed for iron ions as a large fraction of them are mainly located on the NP surface and are badly coordinated. On the contrary, the removal here of manganese cations from the surface shell should induce an increase of their mean coordination number because Mn cations located in the inner structure of the nanocrystal cores should be mostly well coordinated.[38]

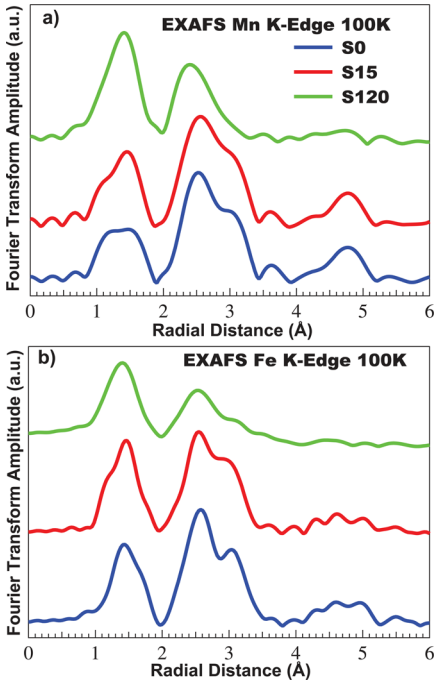

Figure 3. Magnitude of the k^2-weighted Fourier-transformed EXAFS signals taken at 100 K at the (a) Mn K-edge and (b) Fe K-edge for S0, S15, and S120 manganese ferrite samples.

We also observe a second contribution between 2.0 and 3.5 Å with a first peak, more intense at around 2.5 Å, related to single scattering of a large proportion of Mn cations located in octahedral sites and a second one, less intense around 3 Å, related to simple and multiple scattering of Mn cations located at both tetrahedral and octahedral sites. As the surface treatment time increases to 120 min, the ratio between the intensity of the first and the second peaks clearly increases, suggesting migration of Mn cations from A to B sites. Moreover, for sample S120, it is possible to see that the peak associated with the second coordination shell peak is left shifted (lower radial coordinates), probably indicating reduction of the interatomic distances between Mn absorber cations and neighboring metallic ions located in the second coordination layer. It should be related to oxidation of the manganese cations from Mn^{3+} to Mn^{4+} and the consequential reduction of the Mn ionic radius. Figure 3b shows the Fourier transform of the absorption spectra of our samples at the iron K-edge. The first contribution located at around 1.5 Å is associated with peak positions, which measure the interatomic distances between the iron ions and their first nearest neighbors, that is, the oxygen anions in A or B site formation. As the surface treatment time increases, we observe that a shoulder develops on the left side of this first contribution. It could correspond to scattering paths involving iron ions at tetrahedral sites with a shorter Fe−O distance. A partial reverse transfer of Mn ions would accompany this partial transfer of iron ions from B sites to A sites. The second contribution related to the second coordination shell of metallic cations results from two peaks. One is located at lower radial distances and is related to single scattering of Fe^{3+} cations located at B sites. The other one, at larger radial distances, corresponds to single and multiple scatterings of Fe^{3+} cations located at both A and B sites. The ratio between the amplitudes of the latter and the former diminishes, indicating that there is migration of iron ions from

DOI: 10.1021/acs.jpcc.6b09274
J. Phys. Chem. C 2017, 121, 8982−8991

octahedral sites to tetrahedral ones, in accordance with the observations at the Mn K-egde. Moreover, reduction of the amplitude of the second coordination shell observed with increasing surface treatment time could indicate both reduction of the coordination number and increasing local disorder. Indeed, the iron ions localized in the surface shell are likely undercoordinated, and their proportion largely increases with surface treatment duration.

D. Mössbauer Spectroscopy. Figure 4 shows the Mössbauer spectra obtained in the absence and in the presence of an external field (**H** = 7 T) for sample S0.

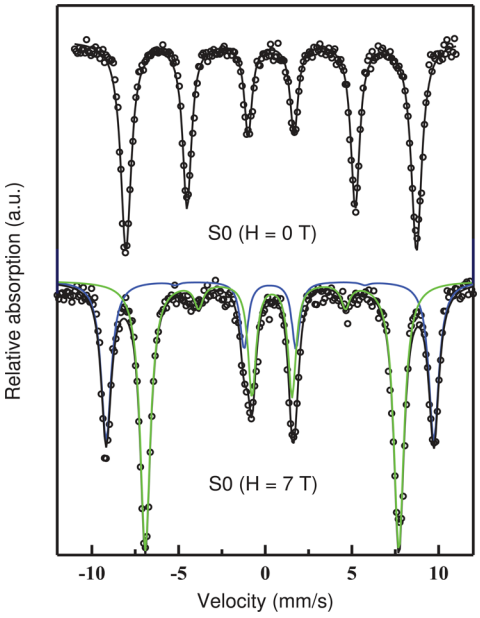

Figure 4. Zero-field and in-field Mössbauer spectra of sample S0 at 4 K. The external field is parallel to the γ-ray axis. The blue line represents the sextet associated with Fe^{3+} ions at A sites, the green one represents the sextet associated with Fe^{3+} ions at B sites, and the black one is the total fit.

The in-field spectrum reveals two distinct features, which are not present in the typical ferromagnetic sextet observed at **H** = 0 for our blocked NPs. The zero-field spectrum is roughly adjusted with one mean hyperfine field at around 51 T. For the in-field spectrum, let us first consider perfect alignment of Fe^{3+} spins. As a consequence of the antiparallel ordering of the spins located at A and B sites, the external lines split into two well-resolved contributions because the external field adds to the magnetic hyperfine field at A sites and subtracts from it at B sites. Second, lines 2 and 5 of these sextets should have vanishing intensities due to a polarization effect because the spins are collinear to the γ-ray direction. In the case of nonperfect alignment of Fe^{3+} spins in the applied field direction, with canting angles at both sites, lines 2 and 5 should have nonzero intensity. The isomer shift, characteristic of the valence state of the Mössbauer absorber atom, takes here typical values obtained for Fe^{3+} ions, therefore indicating that within the uncertainty of our measurements no Fe^{2+} would be present in the NPs' structure. This result will be confirmed by those obtained from LCF analysis of XANES data at the iron K-edge. Then, the in-field spectrum was well fitted using two sextets associated with canted spins of Fe^{3+} ions located at tetrahedral and octahedral polyhedra. From the intensities of each one, we determined the fraction of Fe^{3+} spins tetrahedrally and octahedrally coordinated. The ratio between the intensities of the first and second lines of each sextet was used to obtain the value of the canting angle at each site.[46] We found here an inversion degree equal to 0.72, in good agreement with our NPD results (see the next subsection). The canting angle is negligible at A sites, being inferior to 10° and found slightly larger, at around 17°, at B sites.

E. Rietveld Refinements of NPD and XRD Patterns. Rietveld refinements of NPD and XRD patterns have been performed, as detailed in the SI. For bare NPs (S0), we choose to use δ, the oxidation parameter, as in ref 24, to describe only one structural phase of nonstoichiometric $MnFe_2O_{4+\delta}$ in order to account for both chemical titrations and electroneutrality. According to the former, the metal proportion corresponds to a value of the molar fraction of Mn equal to 0.33 (see Table 1). For the latter, the extra electronegative charge appearing per formula unit exactly compensates for the positive charges coming from the oxidation of Mn ions, leading to $\delta = 0.48$. This approach also corresponds to the following chemical formula unit, $Mn_{0.89}Fe_{1.78}O_4$, and produces both Fe and Mn vacancies in the proportion of 1:2, randomly distributed in both interstitial sites by the fitting procedure. For surface-treated NPs two assumptions have been tested, an only one nonstoichiometric phase and the core−shell model. The details and results (see Figures S3 and S4 and Table S2) are presented in the SI. They clearly indicate for both samples and experiments (NPD and XRD) that the quality and reliability factors are below the acceptable limits seen in the literature[47] and are much better when considering NPs based on a nonstoichiometric Mn ferrite core surrounded by a maghemite surface layer. Only in that case do Figures S3 and S4 show better agreement between calculated and experimental data. We therefore present in the following the Rietveld refinement results of surface-treated NPs obtained by using two spinel phases. Figure 5 shows the NPD pattern of sample S0 fitted by one nonstoichiometric Mn ferrite phase and the Rietveld refinement NPD patterns of samples S15 and S120 taking into account the chemical core−shell model. Table 2 summarizes the structural and magnetic information given by the procedure applied to all samples investigated in this work. The sizes of bare NPs and of CS-NPs taking into account the thickness of the maghemite surface layer are in accordance with those obtained by Scherrer's equation applied to the most intense peak of the XRD pattern (see Table 1). The values obtained for the cubic cell size also reflect good agreement between NPD and XRD behavior. For bare NPs (S0), the size of the lattice cell is smaller when compared to that of the ideal Mn ferrite structure. This is due to the existence of mixed valence states of Mn ions, as will be demonstrated by LCF of XANES data. Then, the smaller average cationic radius[48] induces the reduction of the anion−cation distance and leads to lattice contraction. For CS-NPs, we observe that the longer the surface treatment, the smaller the cubic cell size of the core, this effect being enhanced for sample S120. This is in good agreement with both the larger mean oxidation degree evidenced by XANES and the shift of the diffraction angles observed in the XRD pattern when the surface treatment duration increases.

The lattice cell size of the surface layer structure obtained after 15 min of iron nitrate treatment is larger than that of the ideal maghemite structure (8.356 Å) but very close to the cell size of the core. It seems reasonable as the lattice underlying the whole CS-NP is built during the coprecipitation step. After 120

DOI: 10.1021/acs.jpcc.6b09274
J. Phys. Chem. C 2017, 121, 8982−8991

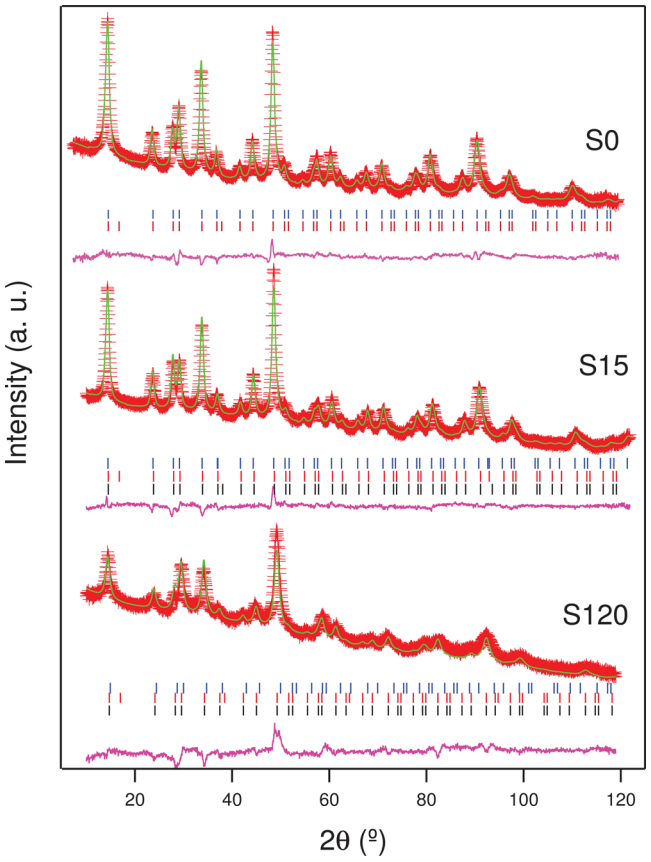

Figure 5. Rietveld refinement of neutron diffractograms of manganese ferrite powder samples, S0, S15, and S120 at room temperature. The experimental points are shown by + symbols, the solid lines are the best fit for the data, and the tick marks show the positions of the allowed reflexions. The lower curves represent the difference between observed and calculated profiles.

min of surface treatment, a contraction of the shell lattice is observed, as that for the core. The value tends to that of maghemite bulk and presents also a very slight mismatch at the core/shell interface. Table 2 also gives the inversion degree, which is found to be equal to 0.667(5) for sample S0. It indicates an average of 3.7 manganese ions per cubic cell migrated from A to B sites when compared to the ideal Mn ferrite structure where x = 0.2. Such rather large values have also been observed by several studies performed on NPs obtained by soft chemistry methods.[22−26] The LCF of XANES data (see the LCF results in the SI, in the Experimental data fits section), which show that 69% of Mn cations present mixed 3+ and 4+ valence states, confirm the strong affinity of these cations to be found at octahedral sites. A surface treatment of 15 min does not change significantly the cation distribution among the spinel sites. The value of the inversion degree for sample S15 is very close to that obtained for sample S0 (difference inferior to 3%), and we observe that only a small fraction, inferior to 5%, of Mn^{3+} oxidizes to Mn^{4+}. However, the inversion degree found for NPs surface-treated for 120 min is much larger, with 82% of Mn cations located at B sites. It indicates that as the surface treatment increases to 120 min more manganese ions are oxidized (see the LCF results in SI, in the Experimental data fits section) and migrate more easily from tetrahedral to octahedral sites, thus increasing the inversion degree.

We also verify from Table 2 that the oxygen position for all samples does not correspond to the value associated with a perfect cubic close-packed structure, u = 0.25. This observation is common in the spinel ferrite structures because the difference in the ionic radius of each cation can easily promote distortions in the oxygen position. Here, the cation−oxygen distance is reduced as a consequence of the existence of mixed valence states of Mn cations in the core, and this also would slightly modify the oxygen position. The magnetic moment obtained at room temperature for both sublattices is refined from typical input values equal to $4.33\mu_B$ and $-3.78\mu_B$, μ_B being the Bohr magneton, at A and B sites, respectively.[49] The values that we found, in good accordance with those of the literature,[25,50] are associated with only one ordered magnetic phase, which accounts here for the Mn ferrite core surrounded by the maghemite surface layer. It could explain the slight increase observed for sample S15. The decrease of the individual A and B site magnetic moments obtained for the S120 sample indicates that a long surface treatment would enhance either the magnetic disorder or the structural and thermal disorder. Our following EXAFS results will enlighten this issue. The results of Rietveld refinement of XRD diffractograms are presented in the SI in Figure S6 in the case of the two tested assumptions about the NP composition. In the best core−shell configuration, they also point out the reduction of the cell size of the cubic spinel lattice underlying the NPs' core induced by the oxidation of Mn ions.

DISCUSSION

We propose here a deeper insight into the detailed structure of the pure manganese ferrite and core−shell $MnFe_2O_{4+\delta}$@γ-Fe_2O_3 NPs that we synthesize. As pointed out by the qualitative analysis of our XAS results, the mean oxidation degree of manganese ions and their location at interstitial sites of the nanocrystal structure are not those of an ideal Mn ferrite structure. Both are also modified by the surface treatment duration. In the following, quantitative analysis of XANES data crossed with the results deduced from NPD, in-field Mössbauer spectroscopy, XRD, and EXAFS will underline the relation between the valence state of manganese ions and the nonequilibrium cation distribution.

As XRD analysis detects only one spinel structure, Mn^{3+} and Mn^{4+} cations are not present as a separate phase but must be located at the sites of the NPs' spinel structure. The mean

Table 2. Structural Parameters Obtained from Rietveld Refinement of the NPD Pattern[a]

aample	D_{NPD} (nm)	e (nm)	a_{core} (Å)	a_{shell} (Å)	x	u_{core}	u_{shell}	μ_B(A) (JT^{-1})	μ_B(B) (JT^{-1})
S0	11.1		8.466(5)		0.667(5)	0.258 (1)		4.47(5)	−3.61(4)
S15	11.2	0.5	8.427(1)	8.415(2)	0.684(7)	0.258(4)	0.256(1)	4.92(7)	−3.65(5)
S120	9.5	0.9	8.328(3)	8.352(5)	0.82(1)	0.256(4)	0.258(1)	3.6(2)	−3.5(1)

[a] D_{NPD} is the particle size, e is the thickness of the maghemite layer, a is the lattice parameter, x is the inversion degree, u is the oxygen position, and μ_B(A) and μ_B(B) are the individual A and B site magnetic moments.

DOI: 10.1021/acs.jpcc.6b09274
J. Phys. Chem. C 2017, 121, 8982−8991

oxidation degree of Mn ions also increases with the duration of the hydrothermal treatment with ferric nitrate, indicating that more Mn cations are oxidized in the Mn ferrite core. We have therefore used the LCF approach to check the proportions of Mn^{2+}, Mn^{3+}, and Mn^{4+} in each sample and to follow the modifications induced by NP surface treatment of these mixed valence states.[24]

The results presented and summarized in Table 3 indicate a combination of valence states that should be attributed to the

Table 3. Results for Inversion Degree x Obtained by NPD (x_{NPD}), Mössbauer Spectroscopy (x_{Moss}), and EXAFS (x_{EXAFS}) showing the % of Mn for All Samples with Valence States 2+, 3+, and 4+

sample	x_{NPD}	x_{Moss}	x_{EXAFS}	% of Mn^{2+}	% of Mn^{3+}	% of Mn^{4+}
S0	0.667(5)	0.72	0.61	31.0	41.9	27.1
S15	0.684(7)		0.63	31.3	36.4	32.3
S120	0.82(1)		0.82	28.2	25.1	46.7

synthesis method performed in a highly basic medium. Indeed, it has been reported over the last 2 decades[21,25] that it easily promotes the oxidization of Mn^{2+} in Mn^{3+}. More recently, XANES studies of coprecipitated $MnFe_2O_4$ NPs and X-ray photoelectron spectroscopy (XPS) of mixed Zn−Mn ferrite NPs have shown significant amounts of tetravalent Mn cations in Mn-based ferrite NPs.[9,26] It should be considered that the result obtained in our bare NPs is also consistent with the reduced cell size of the $MnFe_2O_4$ phase observed by XRD analysis.

The electroneutrality of the nanocrystal structure is maintained thanks to stoichiometric changes.[51] They could be related to oxygen excess or vacancies of metal cations as the compound must remain electrically neutral. In these NPs synthesized by the soft chemistry method, the existence of cation vacancies would be the most probable because oxygen excess that would occur preferentially in nanomaterials were elaborated using a high-pressure route.[52] The simulations results obtained by LCF of XANES reflect the oxidation of Mn cations as the duration of the surface treatment increases. When considering the nonstoichiometric ferrite as in the case of bare NPs, the δ value of 0.48 approximately corresponds to 1 vacancy of the manganese cation and 2 of iron ions per each 10 cubic spinel cells. These vacancies would be more localized on the surface layer of the NPs due to both the existence of the interface and the spatial confinement at the nanoscale. The same LCF procedure has been performed for our XANES data obtained at the iron K-edge considering the linear combination of iron oxide standards such as FeO, Fe_3O_4, and Fe_2O_3. The results are presented in the SI. For all spectra and within the uncertainty of the experiments and analyses, we only found the presence of Fe^{3+} in the manganese ferrite structure of our NPs. In-field Mössbauer spectroscopy confirms this result through the values found for the isomer shift, associated with the presence of only high-spin Fe^{3+} ions, with no detectable Fe^{2+} ions.

EXAFS fits are presented in the SI together with the obtained interatomic distances. The values obtained for all samples are very close to those of the reference material showing once more that the synthesized NPs crystallize in a spinel-type structure. However, when compared to the values of the standard material, the bond distances between Mn ions either at A or B sites and the first layer of oxygen anions are reduced in sample S0 and decrease more with surface treatment duration. It should be due to the presence of Mn^{3+} and Mn^{4+} in the spinel structure of the jacobsite nanocrystals and the oxidation process induced by the longest treatment. As seen in Table 3, the fraction of Mn^{4+} ions increases by a factor of around 74% during surface treatment of 120 min, and this should affect the Mn−O bond distances, as clearly shown in Table S4 of the SI. The effect occurs independent of the type of sites, therefore indicating that Mn cations would be oxidized at both sites. Moreover, the presence of Mn^{3+} ions in an octahedral environment, favored by the high stabilization energy of the crystal field thanks to the split of the eg orbital degeneracy, creates Jahn−Teller distortions.[24,26,34] It would also influence the interatomic distances between Mn cations at octahedral sites and oxygen anions. The fingerprint of the Jahn−Teller effect in XANES spectra is the presence of a shoulder, well marked at around 6552 eV, as seen in Figure 2, for samples S0 and S15, because the number of Mn^{3+} cations is high. Otherwise, in the spectrum of sample S120, the shoulder is less intense as a consequence of the oxidation process of Mn cations induced by surface treatment with ferric nitrate. In a previous paper,[40] we studied the exchange bias that which manifests itself at the interface between the magnetic ordered core and the spin glass-like (SGL) structure of the disordered surface shell. It depends on the magnetic anisotropy[18] of the core phase. However, investigations of local and cooperative distortions in oxide spinels such as $Mg_{1-x}Cu_xCr_2O_4$ have demonstrated the importance of the Jahn−Teller distortions in the production of exchange bias as the magnetic interactions would be affected by these distortions.[53] In our CS-NPs based on manganese ferrite, we attributed the existence of exchange bias to the presence of uncompensated spins onto the core−shell interface of the NPs. According to the results presented here, it would be interesting in the future to better investigate the influence of Jahn−Teller distortions on the exchange bias properties of our Mn ferrite-based CS-NPs. Table 3 indicates that the surface treatment induces oxidation of more manganese ions. It agrees well with a large proportion of them located at octahedral sites because $Mn^{3+}$and Mn^{4+} have a strong affinity for B sites.[9,34] These conclusions also confirm the qualitative analysis previously presented in the subsection C of EXAFS data at the Mn K-edge.

For all samples, the interatomic distances between iron cations and oxygen anions extracted from the fit of EXAFS spectra at the Fe K-edge are in good accordance with the tetrahedral and octahedral bond distances Fe^{3+}(A)−O and Fe^{3+}(B)−O in cubic spinels obtained from the literature.[9,27,54] This result confirms the presence of only high-spin Fe^{3+} ions into the nanocrystal structure, in excellent agreement with LCF of XANES data at the Fe K-edge and with the isomer shift value deduced from in-field Mössbauer spectroscopy, which both point out the absence of Fe^{2+}. However, these interatomic distances are slightly smaller than the typical values tabulated in oxides. It could be ascribed to the high fraction of iron atoms in superficial sites, which are significantly more disordered than those located in the core structure.

The results obtained for the inversion degree using three different experimental techniques are collected for all samples in Table 3. They correspond to the proportion of Mn cations located at octahedral sites. The values found here by EXAFS data, from 0.61 for sample S0 to 0.82 for sample S120, are in good accordance with those deduced from Rietveld refinement of NPD patterns and confirm the same main features. The

DOI: 10.1021/acs.jpcc.6b09274
J. Phys. Chem. C 2017, 121, 8982−8991

presence of Mn cations at B sites of the spinel-type structure of the NPs' core is clearly related to the existence of mixed valence states as observed in several other works.[20,26,27,55] As expected, it indicates that Mn^{3+} and Mn^{4+} present strong affinity for an octahedral environment.[9,34] Moreover, if after the coprecipitation step more than 60% of Mn ions are located at octahedral sites, it is also clearly shown that this proportion increases to 82% with the oxidation process induced by a longer duration of the hydrothermal surface treatment.

Similar magnetic fluids based on ferrite NPs[35,56] with different kinds of cations always present a nonequilibrium cation distribution. However, manganese cations are peculiar; their low standard reduction potentials allow the presence of mixed valence states. The distribution of manganese ions at interstitial sites of the spinel nanocrystals is intrinsically related to their oxidation degree favored by the synthesis method and the hydrothermal surface treatment.

SUMMARY

CS-NPs based on a manganese ferrite core surrounded by a maghemite shell were synthesized by a coprecipitation step followed by hydrothermal surface treatment with ferric nitrate. We study the structural changes that occur with the duration of the surface treatment by crossing, at each step of the synthesis, long- and short-range experimental investigations performed by XRD, NPD, XAS, and in-field Mössbauer spectroscopy. The results provide coherent details of the local atomic arrangement and clearly show that the NP chemistry and structure are intimately related to the oxidation degree of manganese ions in the NP core. Moreover, the chemical core−shell model of surface-treated NPs has been tested by Rietveld refinement of both XRD and NPD patterns, and the fits present better reliability factors whenever the two spinel phases are taken into account. In this context, our investigations allow the following conclusions. After the coprecipitation step, the valence states of Mn ions are already mixed and a large proportion of Mn^{3+} coexists with smaller fractions of Mn^{2+} and Mn^{4+}. These different oxidation degrees of Mn ions result from the coprecipitation process used to synthesize the NPs, performed in a strongly alkaline medium. When the duration of the surface treatment increases, the proportion of Mn^{4+} ions increases at the expense of mainly the Mn^{3+} fraction but also of a slight amount of Mn^{2+}. The oxidation of Mn cations that induces the existence of mixed valence states has several consequences on the local structure of the CS-NPs. First, it leads to contraction of the lattice cell of nontreated NPs due to reduction of the anion−cation distance as the oxidation degree of Mn cations increases. For surface-treated NPs, the cell size of the core underlying-lattice is also reduced, in a more pronounced way for longer treatment as a larger amount of Mn^{3+} oxidizes to Mn^{4+}. These observations are clearly demonstrated by several qualitative and quantitative results such as the shift of XRD peaks and the reduction of both the cell parameter of the Mn ferrite phase precisely determined by NPD and the Mn−O interatomic distances extracted from EXAFS data. The different oxidation degrees found for Mn cations also manifest themselves through the cation distribution at interstitial sites of the spinel nanocrystal structure. Indeed, Mn^{3+} and Mn^{4+} cations present strong affinity for octahedral coordination symmetry, and it is likely that a large proportion of Mn cations is found at octahedral sites of a nontreated NP structure. Then, the absorption edge displays the signature of the Jahn−Teller effect. With the oxidation process induced by surface treatment, even more Mn ions migrate to octahedral sites, and their proportion varies from around 67% in nontreated NPs up to 82% in CS-NPs surface-treated for a longer time. The existence of mixed valence states of Mn ions as well as the possibility of changing the proportions of these different oxidation degrees by surface treatment offers interesting perspectives for catalytic properties. Accordingly, it would be also important to investigate the surface treatment process and its results on the valence states of others metals.

ASSOCIATED CONTENT

Supporting Information

The Supporting Information is available free of charge on the ACS Publications website at DOI: 10.1021/acs.jpcc.6b09274.

Experimental details and data processing, chemical synthesis and analysis of core−shell nanoparticles, X-ray powder diffraction, X-ray absorption, neutron powder diffraction, in-field Mössbauer spectroscopy, experimental data fits, linear combination fit of X-ray absorption near edge structure spectra in Fe K-edge, Rietveld refinement of X-ray diffractograms, fits of extended X-ray absorption fine structure spectra, and extended X-ray absorption fine structure filtered contributions (PDF)

AUTHOR INFORMATION

Corresponding Author

*E-mail: depeyrot@fis.unb.br. Phone: +55 (61)3107-7781. Fax: +55 (61)3107-7781.

ORCID

Fernando H. Martins: 0000-0001-8231-5927

Jérôme Depeyrot: 0000-0002-1689-573X

Notes

The authors declare no competing financial interest.

ACKNOWLEDGMENTS

This work was supported by the Brazilian agencies CNPq, CAPES, FAP/DF, and FAPESP. We greatly acknowledge the bilateral program between French−Brazilian universities UPMC/France and UnB/Brazil through contracts CAPES/COFECUB N° 714/11 and PICS/CNRS N° 5939/11. The authors are also greatly indebted to LNLS for beamtime obtained on the D12A-XRD1 beamline (X-ray diffraction) and on the D04B-XAFS1 beamline (X-ray absorption) to SPEC/CEA/Saclay for the Mössbauer spectroscopy measurements and also to LLB/CEA/Saclay for the beamtime obtained on diffractometer 3T2.

REFERENCES

(1) Gubin, S. P. *Magnetic Nanoparticles*; Wiley-VCH Verlag GmbH & Co. KGaA, 2009.

(2) Gawande, M. B.; Branco, P. S.; Varma, R. S. Nano-magnetite (Fe_3O_4) as a Support for Recyclable Catalysts in the Development of Sustainable Methodologies. *Chem. Soc. Rev.* **2013**, *42*, 3371−3393.

(3) López-Ortega, A.; Estrader, M.; Salazar-Alvarez, G.; Roca, A. G.; Nogués, J. Applications of Exchange Coupled Bi-magnetic Hard/Soft and Soft/Hard Magnetic Core/shell Nanoparticles. *Phys. Rep.* **2015**, *553*, 1−32.

(4) Asin, L.; Goya, G. F.; Tres, A.; Ibarra, M. R. Induced Cell Toxicity Originates Dendritic Cell Death Following Magnetic Hyperthermia Treatment. *Cell Death Dis.* **2013**, *4*, e596−e5100.

(5) PéRigo, E. A.; Hemery, G.; Sandre, O.; Ortega, D.; Garaio, E.; Plazaola, F.; Teran, F. J. Fundamentals and Advances in Magnetic Hyperthermia. *Appl. Phys. Rev.* **2015**, *2*, 041302.

(6) Espinosa, A.; Di Corato, R.; Kolosnjaj-Tabi, J.; Flaud, P.; Pellegrino, T.; Wilhelm, C. Duality of Iron Oxide Nanoparticles in Cancer Therapy: Amplification of Heating Efficiency by Magnetic Hyperthermia and Photothermal Bimodal Treatment. *ACS Nano* **2016**, *10*, 2436−2446.
(7) Ahmed, M. A.; Okasha, N.; El-Dek, S. I. Preparation and Characterization of Nanometric Mn Ferrite via Different Methods. *Nanotechnology* **2008**, *19*, 065603.
(8) Shao, L.; Ren, Z.; Zhang, G.; Chen, L. Facile Synthesis, Characterization of a $MnFe_2O_4$/Activated Carbon Magnetic Composite and its Effectiveness in Tetracycline Removal. *Mater. Chem. Phys.* **2012**, *135*, 16−24.
(9) Beji, Z.; Sun, M.; Smiri, L. S.; Herbst, F.; Mangeney, C.; Ammar, S. Polyol Synthesis of Non-stoichiometric Mn-Zn Ferrite Nanocrystals: Structural/Microstructural Characterization and Catalytic Application. *RSC Adv.* **2015**, *5*, 65010−65022.
(10) Bhosale, R. R.; Shende, R. V.; Puszynski, J. A. Thermochemical Water-splitting for H_2 Generation Using Sol-gel Derived Mn-ferrite in a Packed bed Reactor. *Int. J. Hydrogen Energy* **2012**, *37*, 2924−2934.
(11) Yang, H.; Zhang, C.; Shi, X.; Hu, H.; Du, X.; Fang, Y.; Ma, Y.; Wu, H.; Yang, S. Water-Soluble Superparamagnetic Manganese Ferrite Nanoparticles for Magnetic Resonance Imaging. *Biomaterials* **2010**, *31*, 3667−3673.
(12) Tromsdorf, U. I.; Bigall, N. C.; Kaul, M. G.; Bruns, O. T.; Nikolic, M. S.; Mollwitz, B.; Sperling, R. A.; Reimer, R.; Hohenberg, H.; Parak, W. J.; Förster, S.; Beisiegel, U.; Adam, G.; Weller, H. Size and Surface Effects on the MRI Relaxivity of Manganese Ferrite Nanoparticle Contrast Agents. *Nano Lett.* **2007**, *7*, 2422−2427.
(13) Yang, J.; Lim, E.-K.; Lee, E.-S.; Suh, J.-S.; Haam, S.; Huh, Y.-M. Magnetoplex Based on $MnFe_2O_4$ Nanocrystals for Magnetic Labeling and MR Imaging of Human Mesenchymal Stem Cells. *J. Nanopart. Res.* **2010**, *12*, 1275−1283.
(14) Boni, A.; Marinone, M.; Innocenti, C.; Sangregorio, C.; Corti, M.; Lascialfari, A.; Mariani, M.; Orsini, F.; Poletti, G.; Casula, M. F. Magnetic and Relaxometric Properties of Mn Ferrites. *J. Phys. D: Appl. Phys.* **2008**, *41*, 134021.
(15) Makridis, A.; Topouridou, K.; Tziomaki, M.; Sakellari, D.; Simeonidis, K.; Angelakeris, M.; Yavropoulou, M. P.; Yovos, J. G.; Kalogirou, O. In Vitro Application of Mn-ferrite Nanoparticles as Novel Magnetic Hyperthermia Agents. *J. Mater. Chem. B* **2014**, *2*, 8390−8398.
(16) Vamvakidis, K.; Katsikini, M.; Sakellari, D.; Paloura, E. C.; Kalogirou, O.; Dendrinou-Samara, C. Reducing the Inversion Degree of $MnFe_2O_4$ Nanoparticles Through Synthesis to Enhance Magnetization: Evaluation of Their 1H NMR Relaxation and Heating Efficiency. *Dalton Trans.* **2014**, *43*, 12754−12765.
(17) Lavorato, G. C.; Peddis, D.; Lima, E.; Troiani, H. E.; Agostinelli, E.; Fiorani, D.; Zysler, R. D.; Winkler, E. L. Magnetic Interactions and Energy Barrier Enhancement in Core/Shell Bimagnetic Nanoparticles. *J. Phys. Chem. C* **2015**, *119*, 15755−15762.
(18) Cabreira-Gomes, R.; Silva, F. G.; Aquino, R.; Bonville, P.; Tourinho, F.; Perzynski, R.; Depeyrot, J. Exchange Bias of $MnFe_2O_4$@γ-Fe_2O_3 and $CoFe_2O_4$@γ-Fe_2O_3 Core/Shell Nanoparticles. *J. Magn. Magn. Mater.* **2014**, *368*, 409−414.
(19) Lee, J.; Jang, J.; Choi, J.; Moon, S.; Noh, S.; Kim, J.; Kim, J.; Kim, I.; Park, K.; Cheon, J. Exchange-Coupled Magnetic Nanoparticles for Efficient Heat Induction. *Nat. Nanotechnol.* **2011**, *6*, 418−422.
(20) Tangcharoen, T.; Klysubun, W.; Kongmark, C.; Pecharapa, W. Synchrotron X-ray Absorption Spectroscopy and Magnetic Characteristics Studies of Metal Ferrites (metal = Ni, Mn, Cu) Synthesized by Sol-gel Auto-Combustion Method. *Phys. Status Solidi A* **2014**, *211*, 1903−1911.
(21) Carta, D.; Casula, M. F.; Mountjoy, G.; Corrias, A. Formation and Cation Distribution in Supported Manganese Ferrite Nanoparticles: an X-ray Absorption Study. *Phys. Chem. Chem. Phys.* **2008**, *10*, 3108−3117.
(22) Kravtsov, E.; Haskel, D.; Cady, A.; Yang, A.; Vittoria, C.; Zuo, X.; Harris, V. G. Site-specific Local Structure of Mn in Artificial Manganese Ferrite Films. *Phys. Rev. B: Condens. Matter Mater. Phys.* **2006**, *74*, 104114.
(23) Yang, A.; Chen, Z.; Geiler, A. L.; Zuo, X.; Haskel, D.; Kravtsov, E.; Vittoria, C.; Harris, V. G. Element- and Site-specific Oxidation State and Cation Distribution in Manganese Ferrite Films by Diffraction Anomalous Fine Structure. *Appl. Phys. Lett.* **2008**, *93*, 052504.
(24) Denecke, M. A.; Gunßer, W.; Buxbaum, G.; Kuske, P. Manganese Valence in Precipitated Manganese Ferrite. *Mater. Res. Bull.* **1992**, *27*, 507−514.
(25) Zhang, Z. J.; Wang, Z. L.; Chakoumakos, B. C.; Yin, J. S. Temperature Dependence of Cation Distribution and Oxidation State in Magnetic Mn - Fe Ferrite Nanocrystals. *J. Am. Chem. Soc.* **1998**, *120*, 1800−1804.
(26) Yang, A.; Chinnasamy, C. N.; Greneche, J. M.; Chen, Y.; Yoon, S. D.; Chen, Z.; Hsu, K.; Cai, Z.; Ziemer, K.; Vittoria, C.; Harris, V. G. Enhanced Néel Temperature in Mn Ferrite Nanoparticles Linked to Growth-rate-induced Cation Inversion. *Nanotechnology* **2009**, *20*, 185704.
(27) Carta, D.; Casula, M. F.; Floris, P.; Falqui, A.; Mountjoy, G.; Boni, A.; Sangregorio, C.; Corrias, A. Synthesis and Microstructure of Manganese Ferrite Colloidal Nanocrystals. *Phys. Chem. Chem. Phys.* **2010**, *12*, 5074−5083.
(28) Carpenter, E. E.; O'Connor, C. J.; Harris, V. G. Atomic Structure and Magnetic Properties of $MnFe_2O_4$ Nanoparticles Produced by Reverse Micelle Synthesis *J. Appl. Phys.* **1999***85*.517510.1063/1.369115
(29) Mahmoud, M.; Hamdeh, H.; Ho, J.; O'Shea, M.; Walker, J. Mossbauer Studies of Manganese Ferrite Fine Particles Processed by Ball-milling. *J. Magn. Magn. Mater.* **2000**, *220*, 139−146.
(30) Kang, J.-S.; Kim, G.; Lee, H. J.; Kim, D. H.; Kim, H. S.; Shim, J. H.; Lee, S.; Lee, H.; Kim, J.-Y.; Kim, B. H.; Min, B. I. Soft X-ray Absorption Spectroscopy and Magnetic Circular Dichroism Study of the Valence and Spin States in Spinel $MnFe_2O_4$. *Phys. Rev. B: Condens. Matter Mater. Phys.* **2008**, *77*, 035121.
(31) Tang, Z. X.; Sorensen, C. M.; Klabunde, K. J.; Hadjipanayis, G. C. Size-dependent Curie Temperature in Nanoscale $MnFe_2O_4$ Particles. *Phys. Rev. Lett.* **1991**, *67*, 3602−3605.
(32) van der Zaag, P. J.; Brabers, V. A. M.; Johnson, M. T.; Noordermeer, A.; Bongers, P. F. Comment on "Particle-size Effects on the Value of T_C of $MnFe_2O_4$: Evidence for Finite-size Scaling. *Phys. Rev. B: Condens. Matter Mater. Phys.* **1995**, *51*, 12009−12011.
(33) Brabers, V. A. M. Comment on "Size-dependent Curie Temperature in Nanoscale $MnFe_2O_4$ Particles. *Phys. Rev. Lett.* **1992**, *68*, 3113−3113.
(34) Chen, J. P.; Sorensen, C. M.; Klabunde, K. J.; Hadjipanayis, G. C.; Devlin, E.; Kostikas, A. Size-dependent Magnetic Properties of $MnFe_2O_4$ Fine Particles Synthesized by Coprecipitation. *Phys. Rev. B: Condens. Matter Mater. Phys.* **1996**, *54*, 9288−9296.
(35) Gomes, J. A.; Sousa, M. H.; Tourinho, F. A.; Aquino, R.; da Silva, G. J.; Depeyrot, J.; Dubois, E.; Perzynski, R. Synthesis of Core-Shell Ferrite Nanoparticles for Ferrofluids: Chemical and Magnetic Analysis. *J. Phys. Chem. C* **2008**, *112*, 6220−6227.
(36) Campos, A. F. C.; Aquino, R.; Tourinho, F. A.; Paula, F. L. O.; Depeyrot, J. Influence of the Spatial Confinement at Nanoscale on the Structural Surface Charging in Magnetic Nanocolloids. *Eur. Phys. J. E: Soft Matter Biol. Phys.* **2013**, *36*, 1−11.
(37) Gomes, J.; Azevedo, G.; Depeyrot, J.; Mestnik-Filho, J.; da Silva, G.; Tourinho, F.; Perzynski, R. $ZnFe_2O_4$ Nanoparticles for Ferrofluids: A Combined XANES and XRD Study. *J. Magn. Magn. Mater.* **2011**, *323*, 1203−1206.
(38) Gomes, J. A.; Azevedo, G. M.; Depeyrot, J.; Mestnik-Filho, J.; Paula, F. L. O.; Tourinho, F. A.; Perzynski, R. Structural, Chemical, and Magnetic Investigations of Core-Shell Zinc Ferrite Nanoparticles. *J. Phys. Chem. C* **2012**, *116*, 24281−24291.
(39) Aquino, R.; Depeyrot, J.; Sousa, M. H.; Tourinho, F. A.; Dubois, E.; Perzynski, R. Magnetization Temperature Dependence and Freezing of Surface Spins in Magnetic Fluids Based on Ferrite

DOI: 10.1021/acs.jpcc.6b09274
J. Phys. Chem. C 2017, 121, 8982−8991

Nanoparticles. *Phys. Rev. B: Condens. Matter Mater. Phys.* **2005**, *72*, 184435.
(40) Silva, F. G.; Aquino, R.; Tourinho, F. A.; Stepanov, V. I.; Raikher, Y. L.; Perzynski, R.; Depeyrot, J. The Role of Magnetic Interactions in Exchange Bias Properties of $MnFe_2O_4$@Fe_2O_3 Core/Shell Nanoparticles. *J. Phys. D: Appl. Phys.* **2013**, *46*, 285003.
(41) Tourinho, F.; Franck, R.; Massart, R.; Perzynski, R. In *Trends in Colloid and Interface Science III*; Bothorel, P., Dufourc, E. J., Eds.; 1989; Vol. *79*.
(42) Tourinho, F. A.; Franck, R.; Massart, R. Aqueous Ferrofluids Based on Manganese and Cobalt Ferrites. *J. Mater. Sci.* **1990**, *25*, 3249−3254.
(43) Aquino, R.; Gomes, J.; Tourinho, F.; Dubois, E.; Perzynski, R.; da Silva, G.; Depeyrot, J. Sm and Y Radiolabeled Magnetic Fluids: Magnetic and Magneto-Optical Characterization. *J. Magn. Magn. Mater.* **2005**, *289*, 431−434.
(44) Teo, B. K. EXAFS: Basic Principles and Data Analysis. 1986.
(45) Carta, D.; Casula, M. F.; Falqui, A.; Loche, D.; Mountjoy, G.; Sangregorio, C.; Corrias, A. A Structural and Magnetic Investigation of the Inversion Degree in Ferrite Nanocrystals $MnFe_2O_4$ (M = Mn, Co, Ni). *J. Phys. Chem. C* **2009**, *113*, 8606−8615.
(46) Sousa, E. C.; Rechenberg, H. R.; Depeyrot, J.; Gomes, J. A.; Aquino, R.; Tourinho, F. A.; Dupuis, V.; Perzynski, R. In-field Mossbauer Study of Disordered Surface Spins in Core/Shell Ferrite Nanoparticles. *J. Appl. Phys.* **2009**, *106*, 093901.
(47) Ko, D.; Poeppelmeier, K.; Kammler, D.; Gonzalez, G.; Mason, T.; Williamson, D.; Young, D.; Coutts, T. Cation Distribution of the Transparent Conductor and Spinel Oxide Solution $Cd_{1+x}In_{2-x}Sn_xO_4$. *J. Solid State Chem.* **2002**, *163*, 259−266.
(48) Database of Ionic Radii, Hosted by the Atomistic Simulation Group in the Materials Department of Imperial College, London. http://abulafia.mt.ic.ac.uk/shannon/radius.php (accessed May 20,2016).
(49) Hastings, J. M.; Corliss, L. M. Neutron Diffraction Study of Manganese Ferrite. *Phys. Rev.* **1956**, *104*, 328−331.
(50) Solano, E.; Perez-Mirabet, L.; Martinez-Julian, F.; Guzmán, R.; Arbiol, J.; Puig, T.; Obradors, X.; Yañez, R.; Pomar, A.; Ricart, S.; Ros, J. Facile and Efficient One-pot Solvothermal and Microwave-assisted Synthesis of Stable Colloidal Solutions of $MnFe_2O_4$ Spinel Magnetic Nanoparticles. *J. Nanopart. Res.* **2012**, *14*, 1−15.
(51) Jasinski, J.; Pinkerton, K.; Kennedy, I.; Leppert, V. Surface Oxidation State of Combustion-synthesized γ-Fe_2O_3 Nanoparticles Determined by Electron Energy Loss Spectroscopy in the Transmission Electron Microscope. *Sens. Actuators, B* **2005**, *109*, 19−23.
(52) Saratovsky, I.; Wightman, P. G.; Pastén, P. A.; Gaillard, J. F.; Poeppelmeier, K. R. Manganese Oxides: Parallels between Abiotic and Biotic Structures. *J. Am. Chem. Soc.* **2006**, *128*, 11188−11198.
(53) Shoemaker, D. P.; Seshadri, R. Total-scattering Descriptions of Local and Cooperative Distortions in the Oxide Spinel $Mg_{1-x}Cu_xCr_2O_4$ With Dilute Jahn-Teller Ions. *Phys. Rev. B: Condens. Matter Mater. Phys.* **2010**, *82*, 214107.
(54) Tailhades, P.; Rousset, A.; Bendaoud, R.; Fert, A.; Gillot, B. Structural Study of New Manganese Defect Ferrites. *Mater. Chem. Phys.* **1987**, *17*, 521−529.
(55) Makovec, D.; Kodre, A.; Arčon, I.; Drofenik, M. Structure of Manganese Zinc Ferrite Spinel Nanoparticles Prepared With Co-precipitation in Reversed Microemulsions. *J. Nanopart. Res.* **2009**, *11*, 1145−1158.
(56) Deepak, F. L.; Bañobre López, M.; Carbó-Argibay, E.; Cerqueira, M. F.; Piñeiro Redondo, Y.; Rivas, J.; Thompson, C. M.; Kamali, S.; Rodríguez-Abreu, C.; Kovnir, K.; Kolen'ko, Y. V. A Systematic Study of the Structural and Magnetic Properties of Mn-, Co-, and Ni-Doped Colloidal Magnetite Nanoparticles. *J. Phys. Chem. C* **2015**, *119*, 11947−11957.

DOI: 10.1021/acs.jpcc.6b09274
J. Phys. Chem. C 2017, 121, 8982−8991